This is an *Accepted Manuscript*, which has been through the Royal Society of Chemistry peer review process and has been accepted for publication.

Accepted Manuscripts are published online shortly after acceptance, before technical editing, formatting and proof reading. Using this free service, authors can make their results available to the community, in citable form, before we publish the edited article. We will replace this *Accepted Manuscript* with the edited and formatted *Advance Article* as soon as it is available.

You can find more information about *Accepted Manuscripts* in the **Information for Authors**.

Please note that technical editing may introduce minor changes to the text and/or graphics, which may alter content. The journal's standard **Terms & Conditions** and the **Ethical guidelines** still apply. In no event shall the Royal Society of Chemistry be held responsible for any errors or omissions in this *Accepted Manuscript* or any consequences arising from the use of any information it contains.

Dalton Transactions

ARTICLE

A general, eco-friendly synthesis procedure of self-assembled ZnO-based materials with multifunctional properties

Alina Stan,[a] Cornel Munteanu,[a] Adina Magdalena Musuc,[a] Ruxandra Birjega,[b] Ramona Ene,[a] Adelina Ianculescu,[c] Iulia Raut,[d] Luiza Jecu,[d] Mihaela Badea Doni,[d] Elena Maria Anghel,[a] and Oana Carp*,[a]

A bioinspired one-pot approach for the synthesis of ZnO - carbohydrate hierarchical architectures was developed. The synergy between a saccharide (mono, di- or polysaccharide) that contains D-glucose units and triethanolamine is the key parameter of the synthetic methodology. The morphology of the ZnO composites is dictated by the used saccharide, and rod, spindle, solid and hollow spherical-like ZnO structures are obtained varying the carbohydrate. The synthesized composites present good photocatalytical and antimicrobial activity.

Introduction

The research community faced up with an unprecedented challenge: environmental protection versus sustainable economic growth. The novel properties of the nanostructures,[1-3] mainly attributed to their size-related effects are put in difficulty by their environmentally unfriendly synthetic protocols.[4] In the last decade, the increased receptiveness towards the environment has promoted the development of "greener" synthetic methodologies,[5] and *what could be greener than saccharides*? Their genuine "green" attributes (nontoxic nature, highly availability and renewability) associated with their exceptionally versatile functionalities permit to build an environmentally friendly chemistry of materials (metals, oxides, composites). Indubitable, the added value brought both in terms of material quality and "greening" chemistry is substantial. Although some progress regarding the involvement of saccharides in materials synthesis has been already made, the identification, investigation and development of carbohydrates assisted synthetic routes is (unfortunately) an insufficiently explored research topic of the chemistry.[6-7] Concerning for example metallic oxides, the literature mentions several synthetic methodologies assisted by specific saccharides (glucose but also polysaccharides as dextran, cellulose and its derivatives, chitosan, *etc*.),[6] but an approach with a certain generalization degree is still missing. This is one of the goals of the present research. Following a small steps approach, we selected for the start mono-, di- and polisaccharides having in common the presence of *D*-glucose units (Fig. 1): *(i)* the monosaccharide glucose, *(ii)* the disaccharide sucrose [α-*D*-glucopyranosyl-(1→2)-β-*D*-fructofuranosid], and *(iii)* the polysaccharides starch and dextran containing *D*-glucose units linked by α-glycosidic bonds and, methylcellulose constituted from *D*-glucose units linked by β-bonds. Since sucrose contains

besides a glucosyl unit a fructosyl one, fructose was also included in the tested carbohydrates.

The procedure was tailored for zinc oxide, being known its extraordinary combination of size and shape depended properties (semiconducting, piezoelectric, pyroelectric, optical, antibacterial and (photo)catalytical ones)[8-10], that generate wide range-applications. Additional, ZnO is cheap, nontoxic and biological compatible.[11-13]

The developed one-pot synthetic procedure is eco-friendly both regarding utilized raw materials (zinc acetate as zinc source, the mentioned carbohydrates as growth inhibitors and crystal habit modifiers and triethanolamine -a harmless triol ammine as pH modifier, chelating agent and template), and synthetic methodology (mild hydrothermal procedure carried out at low temperature for a short period of time). The morphology control of the self-assembled ZnO - saccharide superstructures accomplished by a simple variation of the used carbohydrate constitutes the strength of the elaborated "green" procedure. The synthesized materials proved to be feasible for use in photocatalysis and as antimicrobian agents.

Experimental

Materials

All chemicals (analytical grade) were used as received: glucose (Carl Roth GmbH, Germany, G), fructose (Carl Roth GmbH, Germany, F), sucrose (Carl Roth GmbH, Germany, S), dextran (Pharmacia, Denmark, D), soluble oxidized corn starch (Carl Roth GmbH, Germany, ST), methylcellulose (Carl Roth GmbH, Germany, MC), zinc acetate dihydrate (Reactivul, Romania, ZA) and triethanolamine ($N(C_2H_4OH)_3$, Reactivul, Romania, TEA).

Dalton Transactions

ARTICLE
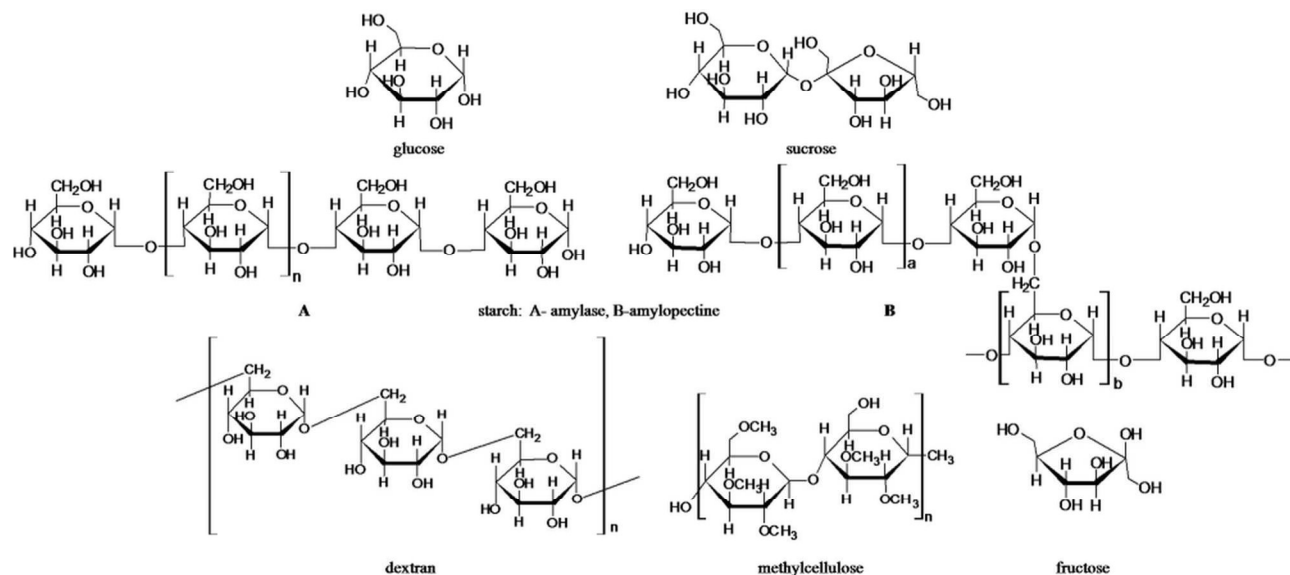
Fig 1. Molecular formula of the tested saccharides.

Synthesis procedure

The hydrothermal synthesis of ZnO / saccharide composites was performed using zinc acetate, saccharides (SAC) and triethanolamine in a molar ratio ZA : SAC : TEA = 1 : 2 : 2 (for polysaccharides the repeating units are considered SAC molecular mass). In a typical procedure, 2 mmol of SAC and 1 mmol of ZA were dissolved together in 40 ml distilled water and after a magnetically stirring of 15 minutes, 2 mol of TEA was added (pH is ~6.5-7). Afterward, the solution was placed in a 45 mL capacity Teflon-lined stainless steel autoclave and heated in an oven at 120 °C for 2 h. The products were filtered off, washed several times with distilled water and finally dried at 70 °C for 10 h. The samples were noted ZnO_SAC where SAC represents the corresponding saccharide. The control sample obtained in the absence of saccharides is noted as ZnO. *Observation*: because in ZnO_MC sample the ZnO is embedded into a film-like matrix, it is difficult to use a constant ZnO amount for photocatalytical and antimicrobial investigations; thus, the composite was calcinated at 500 °C / 1h in order to eliminate MC and the calcinated sample is noted ZnO_MC_500.

Characterization

FTIR spectra (KBr pellets, 400 – 4000 cm^{-1}) were recorded with a FTIR Brucker Tensor V-37 spectrophotometer. The UV–Vis spectra (diffuse reflectance technique, 200 - 1800 nm) were obtained with a JASCO V-670 spectrophotometer. Thermal measurements were performed on a Netzsch thermo balance STA 449F1 type, in static air, with a heating rate of 5 °C / min and a sample mass of ~5 mg. X-ray diffraction measurements were carried out at room temperature with a PANalytical

X'Pert MPD diffractometer, using Ni-filtered CuKα radiation (λ = 1.5418 Å), with a scan step of 0.02° and a counting time of 20 sec / step, for 2θ ranged between (20 – 80)°. The average crystallite size (D) of the samples were determined using the Williamson-Hall equation $\beta_{hkl} \cos\theta_{hkl} = k\lambda/D + 4\varepsilon \sin\theta_{hkl}$, where λ is the wavelength of the CuK_α radiation, k a constant equal to 0.9 and β_{hkl} the instrumental corrected broadening measured at half-maximum intensity of the (hkl) peak at θ_{hkl} Bragg diffraction angle. From the plot of $\beta_{hkl}\cos\theta_{hkl}$ vs $4\sin\theta_{hkl}$ one can evaluate the contribution of the microstrain and crystallite size: from the intercept of the linear fit curve with the ordinate the average crystallite size is extracted, and from the slope of the line the microstrain ε is obtained. The HighScore Plus powder diffraction software from PANlaytical using the Rietveld method was utilized for the evaluation of the lattice parameters. In order to analyze the oxides particles morphology, scanning electron microscopy (SEM) images using a FEI - Quanta 3D FEG Dual Beam and a Quanta Inspect-F were taken. Photoluminescence (PL) measurements were performed on a JASCO FP 6500 spectrophotometer, using 350 nm excitation line of xenon light. Unpolarized solid state Raman spectra (50 - 4000 cm^{-1}) were recorded by means of a Jobin-Yvon–Horiba LabRam HR 800 spectrometer. The 514 nm line of an Ar^+ laser was used as exciting radiation, and the diameter of the laser spot of ~0.7 μm on the sample surface provided a spectral resolution better than 2 cm^{-1}. The resulted spectra were polynomial corrected for background and curve fitted by Lorenzian profile by using Igor software. Low incident power (~1.6 mW) was used to avoid local heating and graphitization effects.

Photocatalytical activity

The photocatalytic activity of the ZnO_SAC composites was evaluated for methylorange (MO) decolorization under UV light (365 nm) irradiation in an aqueous solution of 10^{-5} M concentration. The reaction was conducted in stationary quartz reactors, at room temperature under vigorous stirring without pH adjustment (pH ≈ 6.5). No external oxygen supply was employed. To reach adsorption – desorption equilibrium, the suspensions were magnetically stirred in the dark for 30 min prior to irradiation. The samples collected every hour were immediately centrifuged at 4000 rpm for 10 min, and then filtered through a 0.22 μm millipore filter to remove the used catalyst. The unreacted MO was identified by UV-Vis spectroscopy (Jasco V-570 device) by measuring the absorption intensity at λ_{MO} = 464 nm attributed to the conjugated structure constructed *via* azo bond of MO molecule.[14] The decoloration conversion of MO (η) was calculated using the formula η = (C_0 – C)/C_0x100%, where C_0 and C are the MO concentrations before irradiation and after a certain irradiation time, respectively.

Biocide activity

Both qualitative and quantitative analyses of ZnO_SAC composites actions against Gram-positive and Gram-negative bacterial strains were performed using disc agar diffusion assay (see Electronic Supplementary Material) and optical density (OD_{590}) method. The Gram-negative *Pseudomonas aeruginosa* and the Gram-positive *Bacillus subtilis* 1016 have been selected as model organisms in antibacterial quantitative experiments. The experiments were performed in triplicate under the same conditions and the average values were further used. The bacterial colonies grown on a Luria Bertani (LB) medium were incubated for 48 hours at 37 °C, till a concentration of 1.95 x 10^8 colony forming units per milliliter (CFU/ml) is attained. Flasks containing 50 mL of LB nutrient medium and different amounts of ZnO_SAC composites corresponding to the final concentrations of 50, 100, 200 and 500 μg/ml were subsequently inoculated with 1 mL freshly prepared bacterial suspension and then incubated on an orbital shaker Heidolph Unimax 1010 at 150 rpm at 37 °C for 30 hours. The bacterial growth curves were determined by measuring the time evolution of the optical density (OD) at 590 nm with a spectrophotometer BioMate. As control samples were used LB broth medium cultured under the same conditions and nutrient medium with ZnO_SAC composites.

Results and discussion

Synthesis and characterization of ZnO - saccharide composites

In contrast with other ZnO synthetic methodologies that are performed at high pH with the addition of an alkali excess, in the present approach the ZnO mineralization occurs without additional basic agents such as NaOH, ammonia, *etc.*. On the other hand, the simultaneous presence in the reaction medium of TEA, saccharide and acetate ions complicates the mechanism of ZnO mineralization, because all three have the ability to establish different linkages (electrostatic, coordinative, hydrogen and van der Waals bonds) with Zn^{2+}, polar ZnO crystal and between them as well. The ease and

versatility of TEA molecules for coordination, permits the formation of coordination compounds with different nuclearities (from mononuclear to metallic clusters)[15] in which the amino-alcohol can function as mono-, di- and tridentate ligand. Therefore, it can be assumed that initially, different Zn (II) – TEA complexes are formed. These complexes constitute the Zn^{2+} reservoir, releasing *via* a controlled hydrolysis the metallic cations. Functional ZnO seeds are generated throughout the pioneer stage of the hydrothermal treatment.

The subsequent growth of ZnO particles is strongly influenced by the presence in the reaction medium of the additives that may be adsorbed selectively on specific crystal facets. Consequently, the growth rates of the various crystallographic may be changed, and distinct morphologies are developed.

The representative SEM images of the synthesized ZnO samples are shown in Fig. 2. In the absence of the saccharides, elongated hexagonal rods of variable lengths (10 - 20 μm), frequently jointed into bunches are obtained (Fig. 2a). Seldom ellipse-like heads are also noticed and, at the middle of every structure, planar defects were observed. The high roughness of the side parts indicates that the ZnO structures are constituted from assembled nanorods (Fig. 2a inset). When glucose is added, hexagonal rods are also obtained. The rods present uniform sizes (average length and width about 9 respectively 3.5 μm) and most of them are ending with successive steps and terraces (Fig. 2b). The lateral surface facets are noticeable smoother, the planar defects at the middle of the structures are not so visible, both parts of the bipods being in most cases symmetrical. Spindle-like ZnO, with an average diameter of the half spindle of ~ 700 nm and an aspect ratio of ~3 are obtained if sucrose is introduced in the synthesis (Fig. 2c). Some of the spindels are joined into bundles. Although most of them presents ellipse-like head structure, well-faceted hexagonal ends are also noticed. The lateral sides are smooth and all structures have a joint boundary perpendicular to the major axis which divides the ellipsoidal morphologies into two symmetrical parts. Single ZnO microspheres with diameters of 60 nm - 1.3 μm have been obtained with starch-assisted synthesis (Fig. 2d). The high magnification SEM image (Fig. 2d inset) clearly shows that ZnO microspheres are solid mesocrystals, with rough external surface, composed from small nanoparticles with sizes of 7 - 13 nm. The dextran assisted experiments lead to uniform spindle-like morphologies (length = 2.5 - 3.2 μm and maxima diameters of the half spindle = 650 - 830 nm) characterized by a rough surface on which the constituent rods are identified (Fig. 2e). A bottlenecked joint boundary which links the ellipsoidal structures is also identified. In the case of methylcellulose derived oxide the SEM analysis was performed only for the calcinated sample to reduce the charge effects during the electronic beam approximation to the organic substrate. ZnO_MC_500 sample is present as uniform hexagonal rods with lengths of 3 – 3.30 μm and an aspect ratio of ~3 - 3.5, whose surfaces present erosion traces ((Figure 2f). In the case of fructose, irregular, spherulitic morphologies (with a diameter ranging from 370 – 950 nm) are formed (Figure 2g). A higher magnification of the SEM image (Figure 2g inset) identified hollow spaces inside of the sphere-like architectures due to a radial arrangement of successive bent rows of prismatic or cubic crystallites that composed the outer shell with an average thickness of ~230 nm.

Dalton Transactions

ARTICLE
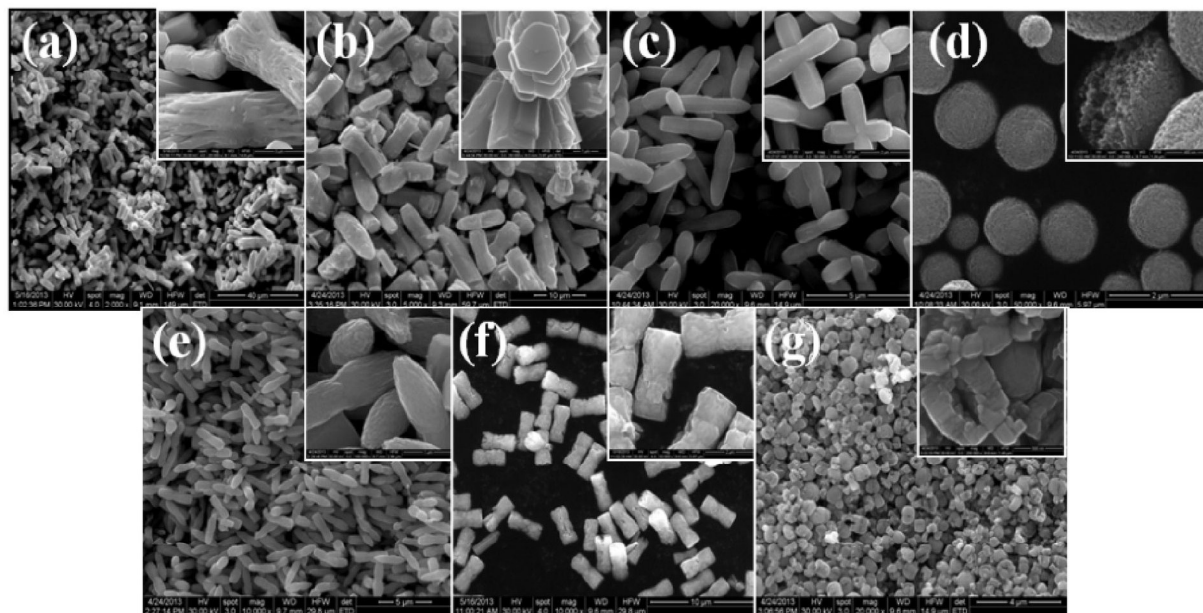
Fig. 2 SEM images of: (a) ZnO; (b) ZnO_G; (c) ZnO_S; (d) ZnO_ST; (e) ZnO_D; (f) ZnO_MC_500; (g) ZnO_F.

All obtained ZnO-saccharide composites exhibits the ZnO-wurtzite structure (hexagonal phase, space group P6$_3$mc) (Fig. 3, Table 1). No impurities have been detected with the exception of sample ZnO_MC for which the broad peak around 20º (see the inset in Fig. 3) known as the "amorphous hump" indicates the presence of methylcellulose. In spite of the variety of morphologies displayed by the samples, their crystallographic data, lattice parameters and tetragonality ratios are almost similar and quite close to the standard ZnO - zincite (JCPDS 36-1451). However, a preferred orientation along the [100] axe revealed by the significant higher ratios of the

intensities corresponding to the (100) and (002) reflections (I_{100}/I_{002}) in comparison with the standard is observed. Samples ZnO_G, ZnO_S, ZnO, ZnO_MC_500 exposing rod-like or spindle-like morphologies with higher aspect ratios, show also the highest I_{100}/I_{002} ratios. ZnO_ST sample with fine typical spherulites morphology exhibits no preferred orientation and has the smallest mean crystallites size.

The IR investigations of the ZnO_carbohydrate composites (Fig. 4) prove the formation of ZnO and the presence of bonded water and carbohydrate (except ZnO_MC_500 in which the carbohydrate is absent).

Table 1. Structural and morphological data of the obtained ZnO_SAC composites.

Sample	Morphology	Lattice parameters			D ±esd (nm)	ε ±esd (x10^{-3})	I_{100}/I_{002}
		a (nm)	c (nm)	c/a			
ZnO (JCPDS 36-1451)	-	0.324982 (15)	0.520661 (15)	1.602	-	-	1.21
ZnO	non-uniform rod	0.3241(6)	0.5195(3)	1.6029	85±0.7	1.48	2.33
ZnO_G	uniform rod	0.3242(4)	0.5193(2)	1.6021	65±0.4	1.92	4.91
ZnO_S	spindle	0.3241(4)	0.5191(3)	1.6016	41±0.4	1.22	3.16
ZnO_ST	solid sphere	0.3233(8)	0.5194(4)	1.6018	33±1.8	2.15	1.27
ZnO_D	spindle	0.3243(7)	0.5179(5)	1.6019	51±2.2	1.09	1.17
ZnO_MC	-	0.3233(8)	0.5182(4)	1.6063	37±2.1	0.31	1.37
ZnO_MC_500	uniform rod	0.3226(7)	0.5190(1)	1.6020	64±0.2	1.14	1.91
ZnO_F	hollow sphere-like architecture	0.3240(3)	0.5188(2)	1.6002	54±2.8	1.42	1.28

Dalton Transactions

ARTICLE
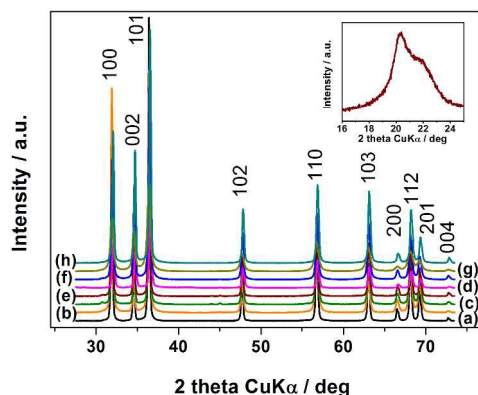
Fig. 3 XRD patterns of: (a) ZnO; (b) ZnO_G; (c) ZnO_S; (d) ZnO_MC_500; (e) and inset ZnO_MC; (f) ZnO_F; (g) ZnO_ST; (h) ZnO_D.

Thus, the broad absorption band with maxima at ~3200 - 3400 cm^{-1} is assigned to chemisorbed and/or physisorbed water molecules and/or hydroxyl groups, and the ones registered in 1500 - 800 cm^{-1} range are characteristic of the used saccharide.
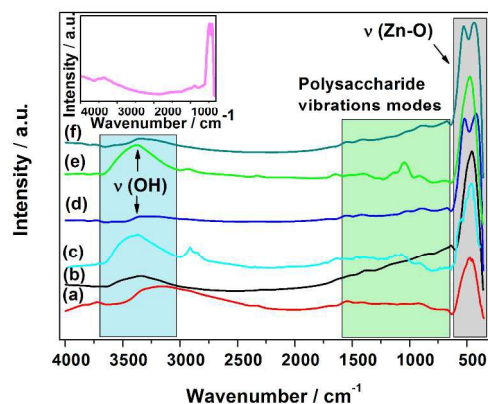
Fig. 4 FTIR spectra of: (a) ZnO_G; (b) ZnO_F; (c) ZnO_MC; (d) ZnO_D; (e) ZnO_ST; (f) ZnO_S; inset ZnO_MC_500.

The existence of a zinc oxide dominant phase is confirmed by the presence of the typical large and very intense absorption at *ca*. 425 - 520 cm^{-1} attributed to the phonon absorptions of the zinc oxide lattice.

An interesting evolution of this band related to the changes in the geometrical shape of ZnO particles is noticed.[16-17] The absence of any splitting in the case of ZnO_ST and ZnO_F samples sustain a spherical or nearby spherical shape of the particles.[18-19] The studies concerned with the morphology dependency have shown that in case of spherical ZnO structures, the calculated as well as measured spectra show one distinct absorption maximum at around 464 cm^{-1}.[20] The same

value is obtained for ZnO_ST, while for ZnO_F the maximum is blue shifted at 445 cm^{-1}. When oxide morphology changes from spherical to a rod/spindle-like shape, the ZnO distinctive band broadens and splits into two maxima, the magnitude of separation increasing with the increase of the aspect ratio of the corresponding structures (ZnO_G < ZnO_MC_500 < ZnO_S < ZnO_D).

The thermal behavior of the obtained ZnO/saccharide composites (Fig. 1 - Electronic Supplementary Material) pointed out the occurrence of a dehydration step corresponding to water elimination followed by a degradative oxidation of the saccharide in one or two decomposition stages. The final decomposition temperature respects the order: ZnO_G (383 ^{o}C) < ZnO_S (437 ^{o}C) < ZnO_D (493 ^{o}C) < ZnO_F (622 ^{o}C) < ZnO_ST (743 ^{o}C) < ZnO_MC (754 ^{o}C).

The Raman spectra of the ZnO composites are shown in Fig. 5, and the deconvolution results within 300 - 700 cm^{-1} range together with the related band assignments are presented in Table 2. The group theory predicts for the ZnO the following lattice optical phonons: $\Gamma_{opt} = 1A_1 + 2B_1 + 1E_1 + 2E_2$, where the A_1 and E_2, polar and nonpolar modes are Raman active.[21-22] The double degenerated E_1 is also Raman active while B branches are inactive.[21]

ZnO_SAC Raman spectra present two dominant first order vibration modes: E_2^{low} and E_2^{high}. The intense and narrow E_2^{low} band (located at about 99 cm^{-1} except the ZnO_MC_500 case where it is shifted to 96 cm^{-1}) is assigned to the zinc sublattice in ZnO.[21,23] The E_2^{high} mode, associated with oxygen displacement, gives an indication about lattice disorder of the ZnO structure, while its asymmetric shape represents the harmonic phonon–phonon interactions.[21,24]

The upshift of the E_2^{high} mode relative to the single crystal position of this mode (437 cm^{-1})[25] is correlated with the presence of a compressive stress (ZnO_D, ZnO_ST), while the downshift is related with a tensile stress (ZnO_MC_500, ZnO_S).[24,26] It is generally agreed that the stress arises from the mismatch of thermal expansion coefficients or the lattice mismatch and distortion of ZnO solid structures.[26] The suppressed peaks positioned at 546 - 564 cm^{-1} and 567 - 582 cm^{-1} attributed to $A_1(LO)$ and $E_1(LO)$ modes are caused by the oxygen defects or oxygen deficient region.[24,27,28] The full width at half maximum (FWHM) values of the E_2^{high} mode ranging from 7 to 11 cm^{-1} (except ZnO_MC_500) points out a good crystal quality of the self-assembled ZnO structures.[29] On the other hand, the sample ZnO_MC_500 presents the largest broadening of the E_2^{high} band (FWHM = 14 cm^{-1}) and $A_1(LO)$ mode (FWHM = 64 cm^{-1}), demonstrating the most defective structure (Table 2). The region of higher wavenumber (Fig. 5B) is dominated by the wide band at about 1147 cm^{-1} originating from the $2A_1(LO)$ and $2E_1(LO)$ modes at the point of the Brillouin zone. The thermal degradation of the methylcellulose implicates the formation of graphitic material traces, as confirmed by presence of the D and G intense bands (1339 and 1598 cm^{-1}).[30] In the absence of a *post-synthesis* thermal heating, the characteristics vibrations of saccharides are identified.

Since the optical properties of nanostructured ZnO are morphological related,[32] the distinct PL behaviors discerned

Dalton Transactions

ARTICLE
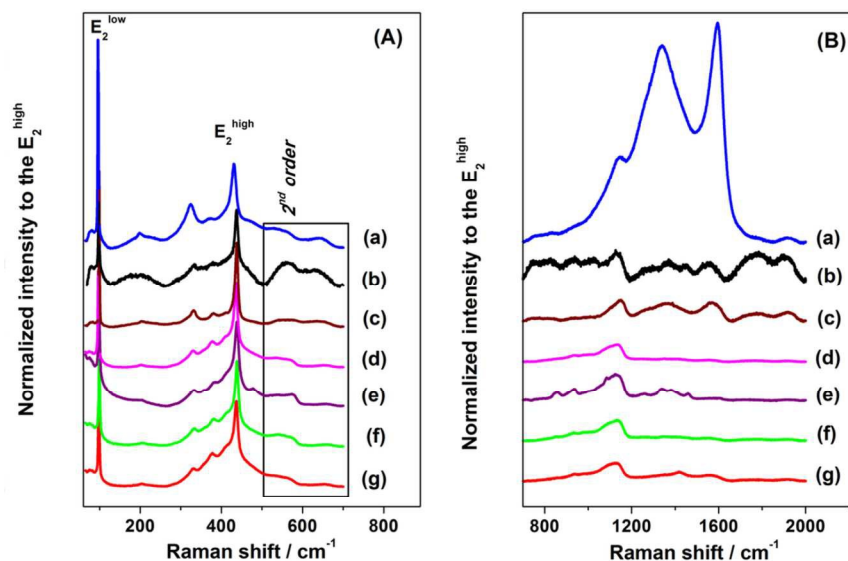
Fig. 5 Raman spectra of: (a) ZnO_MC_500, (b) ZnO_MC, (c) ZnO_F, (d) ZnO_S, (e) ZnO_ST, (f) ZnO_D, (g) ZnO_G samples within (A) 65 - 700 cm^{-1} and (B) 700 - 2000 cm^{-1} spectral ranges.

for the investigated ZnO samples were expected (Fig. 6). Usually, ZnO exhibits emission bands in the UV (attributed to the band-edge transition or exciting combination)[33] and visible (associated with intrinsic or extrinsic defects) regions.[34-35] ZnO_S and ZnO_D samples with a spindle like morphology and relative close sizes, show emissions of approximately equal intensities in the UV, blue and green spectral ranges (the last two assigned to an oxygen deficiency).[35-36] The same emissions are registered for ZnO_ST spherical composite, but their intensities present an ascending trend with wavelength. In the case of rod-like ZnO_MC_500 sample, the UV band is practically absent, but several strong emissions in the indigo domain (quite unusual for ZnO) coupled with a lower green emission band are noticed.

Table 2. Deconvolution results (peak position/FWHM, cm^{-1}), the corresponding chi-square values ($\chi2$) of the fit and the band assignments[21,24,31] of the Raman spectra for ZnO_SAC samples.

ZnO_D	ZnO_G	ZnO_S	ZnO_ST	ZnO_F	ZnO_MC	ZnO_MC_500	Assignment
332/43	329/41	329/40	331/39	330/29	331/43	325/24	E_2^{high}- E_2^{low}
378/45	374/44	375/43	381/58	380/23	377/78	371/55	A_1(TO), ring deformation
-	-	-	-	413/47	-	-	E_1(TO)
422/55	419/57	419/54	423/51	-	423/61	-	$\delta_{(C-C-O)}$
438/9	437/10	436/9	438/11	437/8	437/9	431/14	E_2^{high}
477/74	469/74	472/71	480/40	477/25	464/59	471/79	2LA, ring deformation
536/46	525/59	533/49	534/57	540/41	539/49	527/60	$2B_1^{low}$; 2LA
559/24	546/41	559/26	564/28	560/25	567/60	560/64	A_1(LO)
575/15	567/26	573/15	578/14	579/44	-	-	E_1(LO)
-	-	-	-	629/50	619/76	-	$\upsilon_{(C-C-O)}$, $\delta_{(C-C-O)}$
659/29	651/40	654/38	656/34	655/27	649/51	651/39	TA+LO
0.0315	0.0246	0.0298	0.022	0.0933	0.1314	0.0357	χ^2

Dalton Transactions

ARTICLE
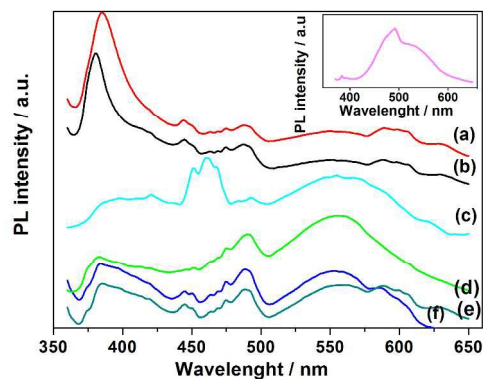
Fig. 6 Room-temperature photoluminiscence spectra of: (a) ZnO_G, (b) ZnO_F, (c) ZnO_MC (inset ZnO_MC_500) (d) ZnO_ST, (e) ZnO_S, (f) ZnO_D.

A surprising resemblance of ZnO_F and ZnO_G spectra was obtained: both consist in a dominant sharp UV band associated with several weak emissions in the visible region (indigo, blue, orange), indication of their good optical properties.[37] As concerning the ZnO_MC composite (Fig. 6 inset), its PL spectrum reveals a low UV peak and a wide but strong emission band covering practically the whole visible range (two maxima in blue-green range), behavior that points out a high density of defects in the sample.[38-39] We have to highlight an unexpected but important conclusion in respect with the green emission, so often encountered for ZnO: our results show that it cannot be related with the reductive character of the saccharide, although it is typically associated with an oxygen deficiency. Glucose and fructose are by far the most reductive saccharides, but their corresponding ZnO based composites do not show any green ranged emissions.
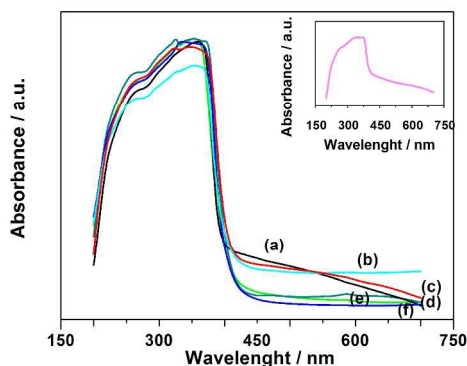
The absorption spectra of the ZnO_SAC composites (Fig. 7) are dominated by a broad and strong band in the exciton absorption region with an absorption band edge onset blue-shifted relative to the bulk (375 nm). This is a result of the size effect and self-assembling in of the discrete nanocrystals in high order structures.[40-41] In the visible region, ZnO_G and ZnO_MC_500 samples show a long tail because of scattering,[42-43] behavior observed for other hierarchical ZnO nanostructures as well.[44] The other composites are not highly transparent in the visible region, suggesting that more absorption states or defect energy bands exist in the as-synthesized ZnO samples,[43] although the contribution of morphological and composition peculiarities cannot be entirely excluded.[43-45]

Photocatalytical activity of the ZnO - saccharide composites

In order to demonstrate the potential of ZnO_SAC composites in environmental applications as the removal of contaminants from wastewater, the photocatalytic degradation of methyl orange (MO) in aqueous solutions under UV irradiation was selected as a model reaction. Preliminary experiments suggest that the photoinduced self-sensitized photolysis of MO could be neglected, the experiments occurring in a pure photocatalytic regime.[46] The temporal evolution of MO decoloration (Fig. 8) highlights that the best photocatalytical efficiency is achieved with ZnO_S and ZnO_D samples (97.6 and 93.5 %). The performance is correlated with the most favorable occurrence of surface defects as types and density in the samples (see Fig. 6), that can act as active centers to capture photo-induced electrons leading to an effective inhibition of photo-induced electrons and holes recombination.[47]

Fig. 7 Absorption spectra of: (a) ZnO_F, (b) ZnO_MC (inset ZnO_MC_500), (c) ZnO_G, (d) ZnO_S, (e) ZnO_ST, (f) ZnO_D.
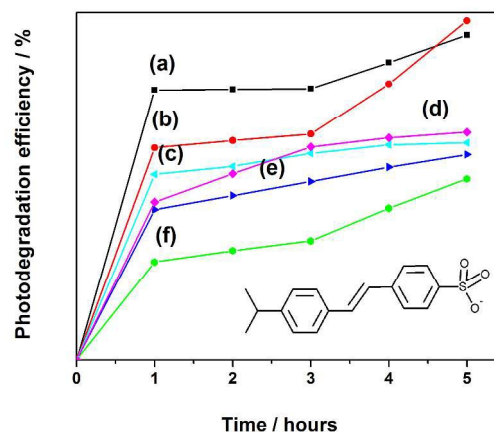
Fig. 8 Decoloration of MC under UV light irradiation in the presence of: (a) ZnO_D, (b) ZnO_S, (c) ZnO_MC, (d) ZnO_ST, (e) ZnO_G, (e) ZnO_F.

At the other end, ZnO_G and ZnO_F composites present the lowest activity (58.9 and 52.0 %), a predictable behavior considering their low defect density as determined through PL investigations (see Fig. 6).

Antimicrobial activity of the ZnO - saccharide composites

The present scenario in which is recorded an outbreak of the infectious diseases caused by bacteria, and these organisms developed resistance to virtually all antibiotics, challenges researchers to design novel specific biocides to complement conventional antibiotics. In comparison to organic antibacterial agents, inorganic nanoscale materials exhibit an inherent size and morphology dependent antibacterial activity, improved chemical stability, ability to withstand adverse processing conditions and long-lasting action.[48-49] Additional, their low-cost and availability into a wide range of controllable morphologies represent other important assets. In this context, oxides such as TiO_2, MgO, CaO, CeO_2 and ZnO, embody a new alternative of biocidal agents.[48-49]

Preliminary qualitative studies conducted using disc agar diffusion method show that ZnO_SAC composites are active against both Gram positive and Gram negative bacterial strains (Fig. 2 - Electronic Supplementary Material). Qualitative investigations, restricted to a Gram positive (*Bacillus subtilis*) and a Gram negative (*Pseudomonas aeruginosa*) microorganism, were carried out evaluating the growth rate of the selected bacterial strains by OD_{590} measurements using ZnO_SAC composites of different concentrations (Fig. 9 and Fig. 3 - Electronic Supplementary Material). The growth rate of

both bacteria is dependent on ZnO_SAC concentrations, *i.e.*, an increased concentration lead to a higher antibacterial activity. In all investigated cases the minimal inhibitory concentration is low, namely 50 μg/ml. The cells growth of *P. aeruginosa* is totally inhibited only by ZnO_ST, (concentration equal with 500 μg/mL), while *B. subtilis* bacterial growth is completely inhibited by all the samples, except ZnO_ST one. ZnO_D and ZnO_MC_500 composites exhibit a remarkable biocidal activity; a concentration of 50 μg/mL respectively 100 μg/mL being sufficient for a total inhibition of the cells growth.

Two features concerning the toxicity of the investigated samples are worth to be pointed out: *(i)* the registered antimicrobial activity sequence of the ZnO_SAC composites is different for the two bacterial strains and *(ii) B. subtilis* cell culture is significantly more sensitive, demonstrating a reduced resistance to the action of ZnO-based composites.

In general, the sensitivity/resistance of Gram-positive and Gram-negative bacteria towards ZnO does not obey a general rule. Some studies report a stronger antibacterial activity on Gram-positive bacteria,[48,50-51] others on Gram-negative ones[52-53] while others identify an equal inactivation of the two classes of bacteria.[54] Different toxicity mechanisms, dissimilarities in the experimental design of the conducted tests (source of light, pH, concentrations of biocidal agents and bacterial cells, *etc.*)[51,55] and, differences in zinc oxide characteristics (shape and abrasiveness, size, surface area, *etc.*)[49,56,57] represent several reasons of these results.

In our case, a plausible explanation of the different toxicity sequence registered for the two strains may be linked to the
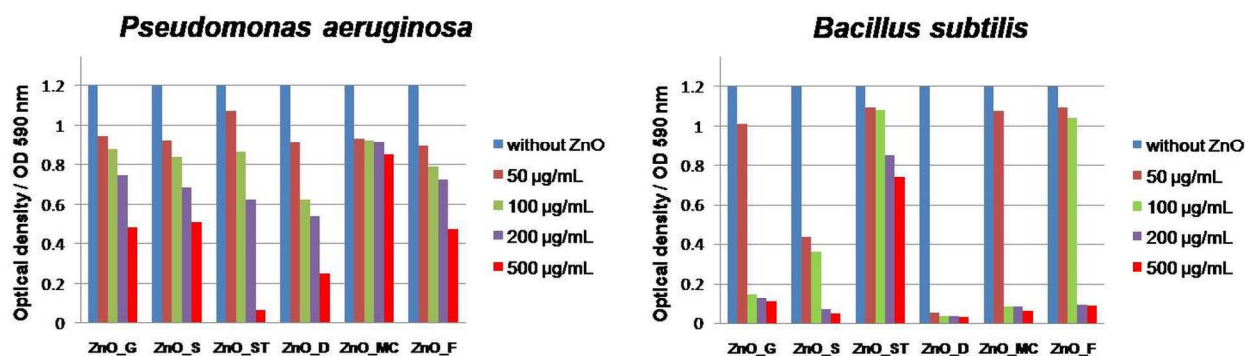
Fig. 9 Grow curves of *P. aeruginosa* and *B. subtilis* in the presence of different concentrations of ZnO_SAC composites (24 hours).

antibacterial mechanism. Three main mechanistic approaches are available in the literature: *(i)* generation of reactive oxygen species (ROS) on the surface of the particles leading to cell death,[58-59] *(ii)* dissolution of ZnO and release of Zn^{2+} ions into the culture,[60-61] *(iii)* ZnO – microorganisms interactions and a subsequent damage the of bacterial cell integrity.[48] The antibacterial activity of the ZnO based samples against Gram-positive *B. subtilis* follows the same trend as their photocatalytic behavior. This means that the biocidal activity is dependent on surface defects presence, and ROS production is the main factor responsible for this biocidal activity. As concerning the mechanism of action against *P. aeruginosa* it is clear that ROS do not play the decisive role.

On the other hand, three other important factors may explain the higher resistance of *P. aeruginosa*: *(i)* the presence of a lipopolysaccharide layer (LPS) layer in Gram-negative bacterial cells that may protect the damage of cell membrane

from toxic molecules,[62] *(ii)* the production of protective extracellular polymeric substances (EPS) that reduces membrane permeabilization,[63] and *(iii)* weaker electrostatic interactions between the bacteria surface and ZnO nanoparticles due to differences in the cell membrane polarity, since the membrane of *P. aeruginosa* is less negative charged than *B. subtilis*[64-65] (the zero charge point of ZnO ranges from 6.9 to 9.8).[66] Other supplementary studies are in progress.

Conclusions

In this work we elaborated a synthetic approach that controls easily, in a "green" context the hierarchical assembling of ZnO structures. The syntheses performed under hydrothermal conditions at 120 °C / 2 hours use two green ingredients, triethanolamine and saccharide (glucose, fructose, sucrose, dextran, starch and methylcellulose). The general

character of the method derives from the possibility of using either mono, di- or polysaccharides that contains D-glucose units. Because the nature of the saccharide rules the construction features of the ZnO structures (rods spindles, hollow and solid spheres), the ability to use various carbohydrates adds to this method a high versatility.

The enhanced photocatalytical and antimicrobial performances indicate the great potential of the ZnO based composites in relevant water detoxification and biomedical applications. Correlating the ZnO_SAC antimicrobial activity with the photocatalytical one, and also with their photoluminescence peculiarities we were able to identify that the mechanism of the biocidal action toward the two investigated bacterial strains follows different paths. An important question that arises is about the role played by the saccharide in the photocatalytical and antimicrobial activity: is it presence beneficial or harmful? At this moment a clear cut answer cannot be given, but certain, their excellent properties for adsorption (contaminants, antibiotics, essential oils, *etc.*) represents positive features.

The proposed approach, alternative to the conventional chemical procedures introduces saccharides as common "chemicals" in the synthesis of high quality oxide materials. Although the full power of the synthetic methodology will be known only after systematic investigations in terms of experimental circumstances, a valuable result related to the eco-friendly chemistry facets of this procedure may be already underlined: biological diversity may be easily used for attaining materials functionality.

Acknowledgements

Notes and references

[a] Romanian Academy, "Ilie Murgulescu" Institute of Physical Chemistry, 202 Spl. Independentei, 060021 Bucharest (Romania)
E-mail: ocarp@icf.ro.
[b] National Institute for Lasers, Plasma and Radiation Physics, 409 Atomistilor, 077125 Magurele (Romania).
[c] University Politehnica of Bucharest, 1-7 Gh. Polizu, 011061 Bucharest (Romania).
[d] National Research and Development Institute for Chemistry and Petrochemistry - ICECHIM 202 Spl. Independentei, 060021 Bucharest (Romania).

1   G. R. Patzke, F. Krumeich and R. Nesper, *Angew. Chem.*, 2002, **114**, 2554; *Angew. Chem. Int. Ed.*, 2002, **41**, 2446.

2   Y. Xia, P. Yang, Y. Sun, Y. Wu, B. Mayers, B. Gates, Y. Yin, F. Kim and H. Yan, *Adv. Mater.*, 2003, **15**, 353.

3   S. Sun, C. B. Murray, D. Weller, L. Folks and A. Moser, *Science,* 2000, **287**, 1989.

4   J. B. Jackson and N. J. Halas, *J. Phys. Chem. B,* 2001, **105**, 2743.

5   M. J. Eckelman, J. B. Zimmerman and P. T. Anastas, J. *Industr. Ecol.*, 2008, **12**, 316.

6   D. Visinescu, G. Patrinoiu, A. Tirsoaga and O. Carp in Environmental Chemistry for a sustainable World (Eds.: E. Lichtfouse, J. Schwarbauer, D. Roberts), Springer, 2013, pp. 119-172.

7   M. Francavilla, A. Pineda, M. Franchi, A. A. Romero Reyes, M. Monteleone, J. C. Colmenares, C. Vargas and R. Luque, *Green Chem.*, 2014, **16**, 2876.

8   S. J. Pearton, D. P. Norton, K. Ip, Y. W. Heo and T. Steiner, *Prog. Mater. Sci.*, 2005, **50**, 293.

9   Z. L.Wang, X. Y. Kong, Y. Ding, P. Gao, W. L. Hughes, R. Yang and Y. Zhang, *Adv. Funct. Mater.*, 2004, **14**, 943.

10   X. F. Zhou, D. Y. Zhang, Y. Zhu, Y. Q. Shen, X. F. Guo, W. P. Ding and Y. Chen, *J. Phys. Chem. B*, 2006, **110**, 25734.

11   P. Nunes, E. Fortunato and R. Martins, *Thin Solid Films*, 2001, **383**, 277.

12   A. J. Freeman, K. R. Poeppelmeier, T. O. Mason, R. P. H. Channg and T. J. Macks, *MRB Bull.*, 2000, **25**, 45.

13   A. P. Alivisatos, *Science,* 1996, **271**, 933.

14   S. H. Liu, S. L. Wang, X. Y. Sun, W. Z. Li, M. Y. Ni, W. F. Wang, M. Wang and S. D. Yao, *Acta Chim. Sinica*, 2004, **62**, 818.

15   E. Conterosito, G. Croce, L. Pallin, E. Boccaleri, W. van der Beek and M. Milanesio, *Cryst. Eng. Comm.*, 2012, **14**, 4472.

16   G.Y. Shan, X. L. Xiao, X. Wang, X. G. Kong, Y. C. Liu and G. Shan, *J. Colloid Interface Sci.*, 2006, **298**, 172.

17   M. Jitianu and D.V. Goia, *J. Colloid Interface Sci.*, 2007, **309**, 78.

18   H. Zhang, R. Wu, Z. Chen, G. Liu, Z. Zhang and Z. Jiao, *Cryst. Eng. Comm.*, 2012, **14**, 1775.

19   M. Bitenc and Z. Crnjak Orel, *Mater. Res. Bull.*, 2009, **44**, 381.

20   M. A. Verge, A. Mifsud and C.J. Serna, *J. Chem. Soc.*, 1990, **86**, 959.

21   R. Cusco, E. Alarcon-Llado, J. Ibanez, L. Artus, J. Jimenez, B.Wang and M. J. Callahan, *Phys. Rev. B*, 2007, **75**, 165202.

22   N. K. Singh, S. Shrivastava, S. Rath and S. Annapoorni, *Appl. Surf. Sci.*, 2010, **257**, 1544.

23   K. F. Lin, H.-M. Cheng, H.-C. Hsu and W.-F. Hsieh, *Appl. Phys. Lett.*, 2006, **88**, 263117.

24   M. Šćepanović, M. Grujić-Brojčin, K. Vojisavljević, S. Bernik and T. Srećković, *J. Raman Spectrosc.*, 2010, **41**, 914.

25   Y. Huang, M. Liu, Z. Li, Y. Zeng and S. Liu, *Mater. Sci. Eng. B*, 2003, **97**, 111.

26   C. Cong, Y. H. Wei, P. F. Zhang, W. Q. Peng, J. J. Wua and X. L. Liu, *Appl. Phys. Lett.*, 2005, **87**, 231903.

27   F. Decremps, J. Pellicer-Porres, A. M. Saitta, J. C, Chervin and A. Polian, *Phys. Rev. B: Condens. Matter Mater. Phys.*, 2002, **65**, 92101.

28   K. Vanheusden, W. L. Warren, C. H. Seager, D. R. Tallant, J. A. Voigt and B. E. Gnade, *J. Appl. Phys.*, 1996, **79**, 7983.

29   Z. X. Li and Y. Xie, *Nanotechnology*, 2005, **16**, 2303.

30   A. Sadezky, H. Muckenhuber, H. Grothe, R. Niessner and U. Pöschl, *Carbon*, 2005, **43**, 1731.

31   M. Łabanowska, A. Wesełucha-Birczyńska, M. Kurdziel and P. Puch, *Carbohydr. Polym.*, 2013, **92**, 842.

Dalton Transactions Accepted Manuscript

32 I. Shalish, H. Temkin and V. Narayanamurte, *Phys. Rev. B,* 2005, **69**, 2454010.

33 L. E. Greene, M. Law, J. Goldberger, F. Kim, J. C. Johnson, Y. Zhang, R. J. Saykally and P. D. Yang, *Angew. Chem. Int. Ed.*, 2003, **42**, 3031.

34 V. A. Dijken, E. Meulenkamp, D. Vanmaekelbergh and A. Meijerink, *J. Phys. Chem. B*, 2000, **104**, 1715.

35 A. B. Djurišić and Y. H. Leung, *Small*, 2006, **2**, 944.

36 Z. Chen, N. Wu, Z. Shan, M. Zhao, S. Li, C. B. Jiang, M. K. Chyu and S. X. Mao, *Scr. Mater.*, 2005, **52**, 63.

37 Z. W. Liu, C. K. Ong, T. Yu and Z. X. Shen, *Appl. Phys. Lett.*, 2006, **88**, 53110.

38 K. Vanheusden, C.H. Seager, W.L. Warren, D.R. Tallant and J.A. Voigt, *Appl. Phys. Lett.*, 1996, **68**, 403.

39 Y. C. Kong, D.P. Yu, B. Zhang, W. Fang and S. Q. Feng, *Appl. Phys. Lett.*, 2001, **78**, 407.

40 Y. C. Zhang, X. Wu, X. Y. Hu and R. Guo, *J. Crystal Growth*, 2005, **280**, 250.

41 D. A. Fleming and M. E. Williams, *Langmuir*, 2004, **20**, 3021.

42 Z. Zhang, M. Lu, H. Xu and W.-S. Chin., *Chem. Eur. J.*, 2007, **13**, 632.

43 T. Ghoshal, S. Kar and S. J. Chaudhuri, *J. Crystal Growth*, 2006, **293**, 438.

44 L. Kumari and W. Z. Li, *Cryst. Res. Technol.*, 2010, **45**, 311.

45 D. Li, I. H. Lueng, B. B. Djurišić, T. Z. Liu, M. H. Xie, S. L. Shi, S. J. Xu and W. K. Chan, *Appl. Phys. Lett.*, 2004, **85**, 1601.

46 B. Haspulat, A. Gülce and H. Gülce, *J. Hazard. Mater.*, 2013, **260**, 518.

47 J. Liqiang, Q. Yichun, W. Baiqi, L. Shudan, J. Baojiang, Y. Libin, F. Wei, F. Honggang and S. Jiazhong, *Sol. Energy Mater. Sol. Cells* 2006, **90**, 1773.

48 R. Brayner, R. Ferrari-lliou, N. Brivois, S. Djediat, M. F. Benedetti and F. Fievet, *Nano Lett.*, 2006, 6, 866.

49 R. Makhluf, Y. Dror, Y. Nitzan, R. Abramovich, A. Jelinek and A. Gevanken, *Adv. Funct. Mater.*, 2005, **15**, 1708.

50 L. K. Adams, D.Y. Lyon and P. J. Alvarez, *Water Res.*, 2006, **40**, 3527.

51 J. Sawai, H. Igarashi, A. Hashimoto, T. Kokugan and M. Shimizu, *J. Chem. Eng. Jpn.*, 1995, **28**, 288.

52 O. N. M. Biebesheimer, A. Zaky and C.L. Gruden, *Environ. Eng. Sci.*, 2010, **27**, 329.

53 R. Sinha, R. Karana, A. Sinha and S. K. Khare, *Bioresour. Technol.*, 2011, **102**, 1516.

54 W. Jiang, H. Mashayekhi and B. Xing, *Environ. Pollut.*, 2009, **157**, 1619.

55 J. Sawai, I. Saito, F. Kanou, H. Igarashi, A. Hasimoto, T. Kokugan and M. Shimizu, *J. Chem. Eng. Jpn.*, 1995, **28**, 352.

56 M. Ramani, S. Ponnusamy, C. Muthamizhchelvan, J. Cullen, S. Krishnamurthy and E. Marsili, *Colloids Surf. B.*, 2013, **105**, 24.

57 O. Yamamoto, M. Hotta, J. Sawai, T. Sasamoto and H. Kojima, *J. Ceramic. Soc. Jpn.*, 1998, **106**, 1007.

58 O. Yamamoto, *Int. J. Inorg. Mater.*, 2001, **3**, 643.

59 G. Applerot, A. Lipovsky, R. Dror, N. Perkas, Y. Nitzan, R. Lubart and A. Gedanken, *Adv. Funct. Mater.*, 2009, **19**, 842.

60 J. Domenech and A. Prieto, *J. Phys. Chem.*, 1986, **90**, 1123.

61 T. Xia, M. Kovochich, M. Liong, L. Mädler, B. Gilbert, H. Shi, J.I. Yeh, J.I. Zink and A.E. Nel, *ACS Nano.*, 2008, **2**, 2121.

62 W. Jiang, A. Saxena, B. Song, B. B. Ward, T. J. Beveridge and S. C. B. Myneni, *Langmuir*, 2004, **20**, 11433.

63 Z. Xue, C. M. Hessler, W. Panmanee, D. J. Hassett and Y. Seo, *FEMS Microbiol. Ecol.*, 2013, **83**, 101.

64 H. Gorna, J. Lawníczak, A. Zgola-Grzoskowiak and E. Kaczouk, *Bioresource Technol.*, 2011, **102**, 3028.

65 G. Pesce, G. Ruisciano, A. Sasso, R. Isticato, T. Sirac and E. Ricca, *Colloids Surf. B*, 2014, **116**, 568.

66 M. Kosmulski in Surfactant Science Series-Chemical Properties of Material Surfaces (Ed. M. Dekker), New York, 2001, vol.102.

Dalton Transactions Accepted Manuscript

A general, eco-friendly synthesis procedure of self-assembled ZnO-based materials with multifunctional properties

Alina Stan,[a] Cornel Munteanu,[a] Adina Magdalena Musuc,[a] Ruxandra Birjega,[b] Ramona Ene,[a] Adelina Ianculescu,[c] Iulia Raut,[d] Luiza Jecu,[d] Mihaela Badea Doni,[d] Elena Maria Anghel,[a] and Oana Carp*,[a]
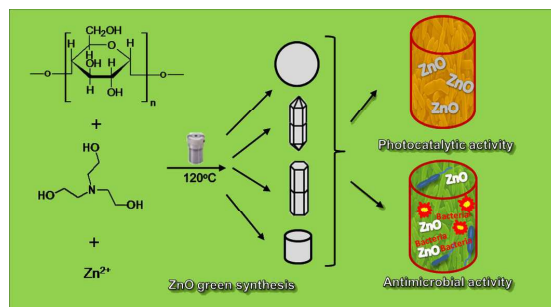
One way of getting green: saccharides in cooperation with triethanolamine are proposed as green and versatile tools for the synthesis of ZnO-based materials with notable photocatalytical and antimicrobian activity.